

Dynamic Nuclear Polarization Enhanced Solid-state NMR Studies of Surface Modification of γ -Alumina

Marco Mais,¹ Subhradip Paul,² Nathan S. Barrow³ and Jeremy J Titman^{1*}

¹School of Chemistry, University of Nottingham, Nottingham, NG7 2RD, UK

²Nottingham DNP MAS NMR Facility, Sir Peter Mansfield Imaging Centre, University of Nottingham, NG7 2RD, UK

³Johnson Matthey Technology Centre, Blounts Court, Sonning Common, Reading, RG4 9NH, UK

*Email: Jeremy.Titman@nottingham.ac.uk

ABSTRACT

Dynamic nuclear polarization (DNP) gives large (>100-fold) signal enhancements in solid-state NMR spectra via the transfer of spin polarization from unpaired electrons from radicals implanted in the sample. This means that the detailed information about local molecular environment available for bulk samples from solid-state NMR spectroscopy can now be obtained for dilute species, such as sites on the surfaces of catalysts and catalyst supports. In this paper we describe a DNP-enhanced solid-state NMR study of the widely used catalyst γ -alumina which is often modified at the surface by the incorporation of alkaline earth oxides in order to control the availability of catalytically active penta-coordinate surface Al sites. DNP-enhanced ^{27}Al solid-state NMR allows surface sites in γ -alumina to be observed and their ^{27}Al NMR parameters measured. In addition changes in the availability of different surface sites can be detected after incorporation of BaO.

Introduction

Solid-state nuclear magnetic resonance (NMR) is a powerful method for studying the molecular structure and dynamics of a broad range of advanced materials. NMR suffers from low sensitivity, because of the small nuclear spin polarizations involved even with high magnetic fields so that long acquisition times or large sample volumes are often required. The problem of sensitivity becomes overwhelming for dilute species, so that measurements of surface sites, molecules at interfaces or isotopes with low natural abundance are often impossible. Fortunately, weak NMR signals can be enhanced by dynamic nuclear polarization (DNP), which involves transfer of electron spin polarization from radicals implanted in the sample to nearby nuclei.¹⁻⁴ This process requires the saturation of the electronic Zeeman transitions at microwave frequencies and is most efficient at low temperatures (<100 K). Until recently DNP has been limited to low magnetic fields because of the lack of high-frequency, high-power microwave sources. However, developments in the design of extended interaction klystrons^{5,6} and gyrotrons⁷ have made DNP spectrometers operating at ¹H NMR frequencies up to 900 MHz possible. Commercial DNP-enhanced solid-state NMR spectrometers have been available since 2010, leading to an increase in publications as shown in Figure 1 illustrating the emergence of DNP, particularly as a surface science technique. The substantial enhancements (routinely >100-fold) obtained with DNP make NMR studies of dilute species feasible for the first time, enabling a >10000-fold time saving, making impossible NMR experiments viable and prompting many new NMR applications, for example, to surfaces.⁸⁻¹³

γ -alumina is widely used as an industrial catalyst support, chosen because of its high surface area, good thermal stability, favourable pore-size distribution and useful acid/base

properties.¹⁴ Catalytically active elements doped onto the support bind to several sites with varying coordination environments at the surface. Pre-treatment of the alumina with alkaline earth and rare earth oxides alters the availability of these different sites, allowing control over the catalytic activity.¹⁵ For example, BaO and La₂O₃ are commonly added as stabilizers to the alumina supports used in three-way catalysts for vehicle emission control.¹⁶

Solid-state ²⁷Al NMR is a powerful technique to characterize the local environment in a wide range of materials, including clays, glasses, zeolites and other microporous systems.¹⁷ ²⁷Al magic-angle spinning (MAS) NMR spectra of transition alumina usually show peaks at approximately 67 and 9 ppm which are assigned to tetrahedrally (AlO₄) and octahedrally (AlO₆) coordinated aluminium, respectively. Surface-selective {¹H} – ²⁷Al cross polarization (CP)^{15,18-21} has revealed a further signal at about 30 ppm which is assigned to fivefold coordinated aluminium sites (AlO₅) in the first surface layer. ²⁷Al MAS NMR of BaO-modified γ-alumina shows a decrease in the proportion of fivefold co-ordinated aluminium as the amount of doping increases,²² suggesting that doping with BaO blocks access to these reactive sites. However, recent computational studies²³ indicate that only a fraction of the surface aluminium may be observed using {¹H} – ²⁷Al CPMAS NMR, since CP favours symmetric sites, although the authors did not account for surface reconstruction²⁴ or for increased motional flexibility at the alumina surface.²² Furthermore, the linewidths of {¹H} – ²⁷Al CPMAS spectra¹⁵ are not narrower than in direct excitation spectra, as would be the case if CP filtered out the response from asymmetric sites.

Hence, the nature of the surface sites of γ -alumina, their modification by other oxides and even the utility of ^{27}Al MAS NMR for studying them are still a matter for debate.

DNP results in surface selectivity because the polarization source is a radical or bi-radical dissolved in a solvent which wets the surface of the sample. At low temperatures the solvent usually forms a glassy matrix, and transfer mechanisms transport the polarization to nuclei in the sample surface. In this case polarization transfer from the biradical to surface ^{27}Al nuclei is achieved by spin diffusion through the dipolar-coupled ^1H network in the frozen organic solvent followed by $\{^1\text{H}\} - ^{27}\text{Al}$ CP. The selectivity means DNP is expected to be an effective method for the study of surface sites in γ -alumina. However, previous DNP-enhanced $\{^1\text{H}\} - ^{27}\text{Al}$ CPMAS spectra of γ -alumina^{21,25} did not show a significant AlO_5 peak, possibly owing to hydration of the surface during the sample preparation. In this paper we describe a new DNP-enhanced $\{^1\text{H}\} - ^{27}\text{Al}$ CPMAS study of γ -alumina and BaO-modified γ -alumina in which a significant AlO_5 peak is observed for the first time with DNP. Sample preparation (see SI) was found to be critical for optimizing the DNP enhancement. It should also be noted that the current study was carried out at higher magnetic field (14.1 T compared to 9.4 T) to provide improved resolution of ^{27}Al environments and with different DNP polarizing agents to previous work.

Results and Discussion

Figure 2 shows the conventional ^{27}Al MAS spectrum of bulk γ -alumina recorded in just 24 s with a total of 24 scans. The signal to noise ratio is very high as expected for a bulk sample, but only two ^{27}Al peaks are observed at approximately 70 ppm and 10 ppm, which can be assigned to the AlO_4 and AlO_6 sites in the γ -alumina structure, respectively.

In order to illustrate the advantages of the method Figure 3 shows (black) the DNP-enhanced $\{^1\text{H}\} - ^{27}\text{Al}$ CPMAS spectra of γ -alumina wetness impregnated with a solution of the biradical TEKPol²⁶ in 1,1,2,2-tetrachloroethane (TCE) as described in the SI. This spectrum shows an extra ^{27}Al peak at about 30 ppm which can be assigned to the surface AlO_5 sites. The lack of significant line broadening with DNP demonstrates that wetting with the radical solution does not have a detrimental effect on the NMR spectrum.

Following convention the DNP-enhanced spectrum (“microwave on”) is compared to an identical one recorded with the gyrotron turned off (the “microwave off” spectrum) (red), and an enhancement ε of 36 can be measured for DNP (see Table S1 in SI) for the AlO_6 site which equates to a 1300-fold saving in time. The surface selectivity of DNP-enhanced $\{^1\text{H}\} - ^{27}\text{Al}$ CPMAS means the AlO_5 site, which is not observed at all in the bulk, is now clearly visible in the spectrum.

The DNP-enhanced ^{27}Al CPMAS spectrum in Figure 3 exhibits lines with a characteristic asymmetric lineshape shape which is evidence of disorder and a distribution of electric field gradients.²⁷ This means that the high-field tail of the asymmetric AlO_5 line overlaps with the AlO_6 peak and two-dimensional experiments are required to improve the resolution and separate them.²⁸ Since ^{27}Al is a quadrupolar nucleus with $I = 5/2$, the approach of choice is the CP-MQMAS (“cross-polarization multiple-quantum MAS”) experiment²⁹ which is described in more detail in the SI. The large signal enhancements obtained with DNP make surface-selective two-dimensional CP-MQMAS experiment feasible. A DNP-enhanced CP-MQMAS spectrum of γ -alumina is shown in Figure 4(A), and the three surface ^{27}Al peaks are clearly resolved. In MQMAS experiments the two-dimensional lineshapes observed depend on the isotropic chemical shift δ_{iso} and

quadrupolar coupling C_Q , as well as the distributions in these parameters arising from disorder. The quadrupolar coupling is determined by the electric field gradient (EFG) which in turn results from the distribution of charges around the observed nucleus.

Czjzek *et al.*^{30,31} derived the joint distribution p of the principal EFG tensor component $V_{zz} = hC_Q/eQ$ and the asymmetry parameter η in the case of a statistical distribution of charges around the observed nucleus

$$p(V_{zz}, \eta) = \frac{V_{zz}^4 \eta}{\sqrt{2\pi} \sigma^5} \left(1 - \frac{\eta^2}{9}\right) \exp \left[-\frac{V_{zz}^2}{2\sigma^2} \left(1 + \frac{\eta^2}{3}\right) \right]$$

where the parameter σ is directly proportional to the average value of the quadrupolar product $P_Q = C_Q(1+\eta/3)^{1/2}$ for the joint distribution. The DNP-enhanced CP-MQMAS spectrum in Figure 4(A) suggests that for the AlO_4 site the distribution in isotropic chemical shift induced by the disorder dominates, since the observed broadening is parallel to the “chemical shift axis” of the two-dimensional spectrum. On the other hand for the AlO_6 site the distribution in the electric field gradient dominates since the observed broadening is along the “quadrupolar induced shift axis” of the two-dimensional spectrum. The interaction between these distributions complicates the interpretation of MQMAS spectra in terms of disorder, so for fitting using the DMFit package³² a Gaussian distribution of isotropic chemical shift is assumed which is uncorrelated with the Czjzek distribution of C_Q . The fit parameters were an amplitude factor, the isotropic position, the width of the Gaussian chemical shift distribution and the average value of P_Q from the Czjzek distribution. Initially, the full DNP-enhanced two-dimensional CP-MQMAS spectrum was fitted, and the chemical shift distribution fixed before fitting the DNP-enhanced MAS spectrum to allow the intensity for each site to be obtained by

integrating over the resulting lineshape. It should be noted that given the complicated polarization transfer mechanisms associated with DNP, $\{^1\text{H}\} - ^{27}\text{Al}$ CP and the MQMAS experiment, this spectrum should be thought of as at best semi-quantitative. Figure 5(A) shows (top) the two-dimensional fit (red) to the spectrum of Figure 4(A) (black), as well as (bottom) the one-dimensional fit (red) to the spectrum of Figure 3 (black). The corresponding fit parameters are given in Table I and these confirm the substantially larger isotropic chemical shift distribution for the AlO_4 site compared to AlO_6 . Wischert *et al.*²³ have demonstrated that $\{^1\text{H}\} - ^{27}\text{Al}$ CPMAS is sensitive to strongly hydrated surface sites and that catalytically important Al centres with high quadrupolar couplings are not always observed, and this might also be the case here.

Figure 6 shows a comparison between DNP-enhanced $\{^1\text{H}\} - ^{27}\text{Al}$ CPMAS spectra of (red) BaO-modified and (black) unmodified γ -alumina (from Figure 3) normalized so that the overall spectral intensity is preserved. It is clear that the AlO_5 peak decreases in intensity while the AlO_4 peak increases after pretreatment with BaO, as found previously by ^{27}Al MAS NMR for BaO ³³ and by $\{^1\text{H}\} - ^{27}\text{Al}$ CPMAS for SrO .¹⁵ This suggests that the reactive surface AlO_5 environment provides a preferential nucleation site for Ba.²²

Figure 4(B) shows a DNP-enhanced CP-MQMAS spectrum of BaO-modified γ -alumina which is similar in appearance to that for unmodified γ -alumina in Figure 4(A). Figure 5(B) shows (top) the two-dimensional fit (red) to the spectrum of Figure 4(B) (black), as well as (bottom) the one-dimensional fit (red) to the BaO-modified γ -alumina spectrum of Figure 6 (black). The results of fitting to the Czjzek model are given in Table I, and the similarity between the parameters obtained for the two samples suggests that modification with BaO does not significantly modify the local environment of the Al

surface sites. However, the width of the distribution of chemical shifts for the AlO_5 site increases with modification by BaO, while $\langle P_Q \rangle$ decreases. This could indicate that BaO adds preferentially to the most distorted AlO_5 sites. In addition to changes in the chemical shift and quadrupolar parameters, the relative intensities confirm that the proportion of AlO_5 sites has decreased after surface modification by BaO, while the proportion of AlO_4 sites has increased.

Conclusions

DNP-enhanced solid-state NMR is an emerging technology for surface science, capable of enhancing surface NMR signals to achieve greater than 1000-fold savings in experiment time. This enabling technology is applicable to many catalyst materials, where structural information about the surface can be critical to the understanding of chemical processes. In the example presented here, bulk NMR measurements of undoped and doped alumina showed no change. However, $\{^1\text{H}\} - ^{27}\text{Al}$ CPMAS NMR of alumina is surface-specific and showed that adding BaO reduced the intensity of the AlO_5 sites. To reveal more insight about the surface environments, two-dimensional CP-MQMAS experiments were required, but these would require prohibitively long experiment times with conventional NMR. Following a novel sample preparation involving grinding in a glovebox prior to radical impregnation, the DNP enhancement obtained was sufficient for acquisition of the required CP-MQMAS spectra in less than 1 day with sufficient signal-to-noise for fitting to structural models. A Czek model revealed the chemical shift and quadrupolar coupling distributions of the three surface environments. These showed little difference between pristine γ -alumina and its BaO-modified counterpart with only a reduction in the intensity of the AlO_5 signal and a concomitant increase for AlO_4 . This

suggests that upon BaO modification the remaining alumina sites are unperturbed by the presence of BaO. These results can be used to refine DFT models of BaO-modified γ -alumina surfaces, to provide insight for further chemical reactions such as doping of metals, or to aid understanding of metal-support interactions and subsequent catalytic testing.

Table I

Czjzek Model Fitting Parameters for Different ^{27}Al Sites^a

$\gamma\text{-Al}_2\text{O}_3$ site	Relative Intensity ^b ± 0.02	δ_{iso} / ppm ^c ± 0.2	Δ / ppm ± 0.3	$\langle P_Q \rangle$ / MHz ± 0.1
AlO ₄	0.10	77.5	16.0	3.5
AlO ₅	0.13	37.2	6.3	4.5
AlO ₆	0.78	14.0	7.2	4.3
BaO/ $\gamma\text{-Al}_2\text{O}_3$ site	Relative Intensity ^b	δ_{iso} / ppm ^c	Δ / ppm	$\langle P_Q \rangle$ / MHz
AlO ₄	0.16	77.4	11.3	4.5
AlO ₅	0.08	34.0	12.7	3.1
AlO ₆	0.76	13.7	7.4	4.2

- errors obtained for each fitting parameters from the DMFit package. Errors quoted are largest obtained for all sites.
- integral over the fitted lineshape. Note that because of the complicated polarization transfer processes associated with DNP, $\{^1\text{H}\} - ^{27}\text{Al}$ CP and MQMAS only the relative intensities within a particular spectrum can be compared.
- isotropic position.

Figures

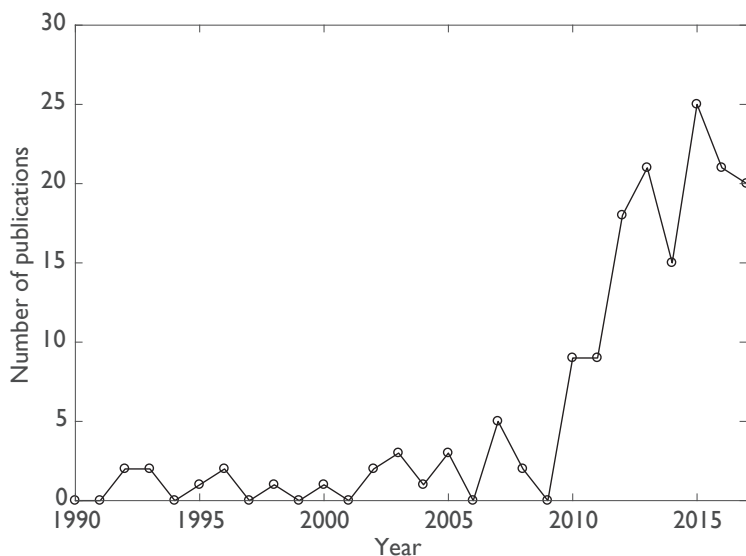


Figure 1. DNP-enhanced solid-state NMR publications by year, based on a Scopus search with the search term TITLE-ABS-KEY((“dynamic nuclear polarization” or “DNP” and “MAS”).

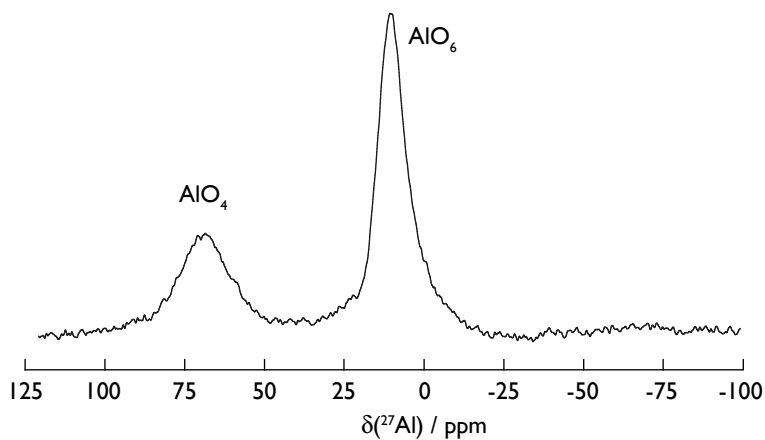


Figure 2. ^{27}Al MAS spectrum of bulk γ -alumina. Two ^{27}Al peaks are present which can be assigned to the AlO_4 and AlO_6 sites in the γ -alumina crystal structure.

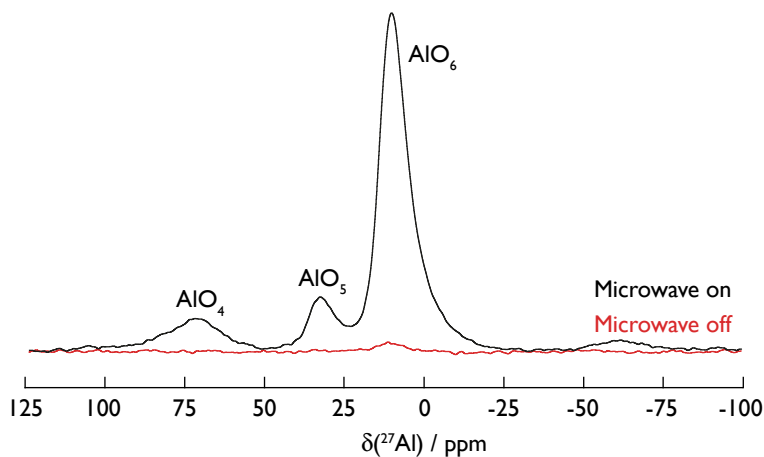


Figure 3. DNP-enhanced $\{^1\text{H}\} - ^{27}\text{Al}$ CPMAS spectrum of γ -alumina (black) and comparison with the corresponding microwave off spectrum (red), showing the 36-fold enhancement obtained in this case using DNP. Note the appearance of a third ^{27}Al peak in the spectrum which can be assigned to the surface AlO_5 sites. Experimental details are given in the SI.

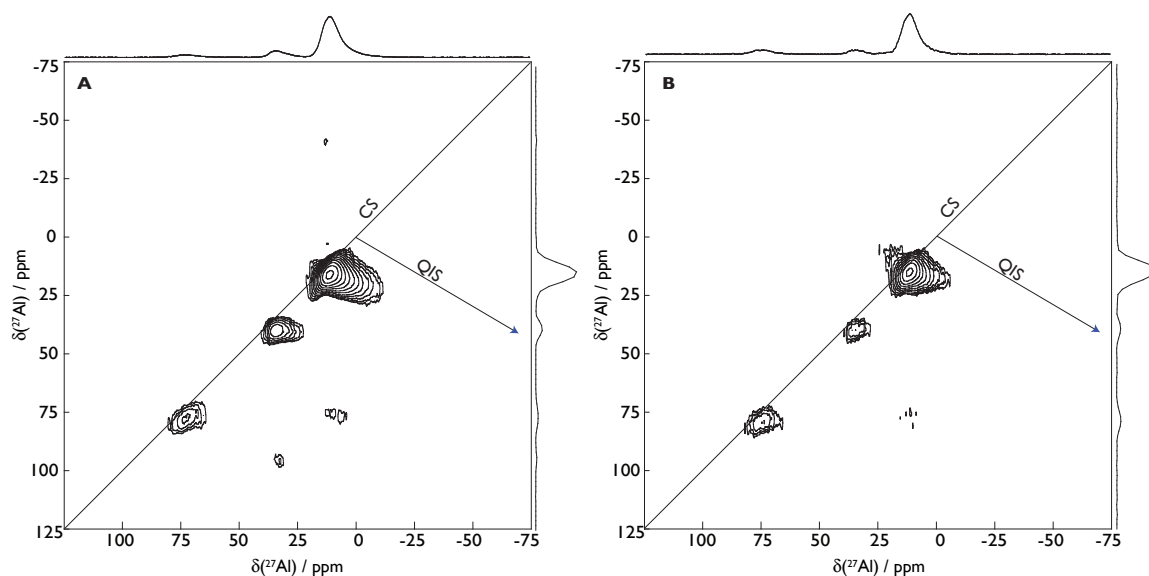


Figure 4. DNP-enhanced two-dimensional $\{^1\text{H}\} - ^{27}\text{Al}$ CP-MQMAS spectra of **A** γ -alumina and **B** BaO-modified γ -alumina. All three ^{27}Al lines are fully resolved in the two-dimensional spectra. There were 100 t_1 increments with 120 co-added scans for each.

Heteronuclear decoupling was applied using the $\text{SW}_f\text{-TPPM}$ sequence with a ^1H rf

amplitude of 90 kHz during t_1 and t_2 . The z-filter delay was 20 μ s. The non-selective ^{27}Al coherence transfer pulse after t_1 was 1.5 μ s in duration with a rf amplitude of 88.6 kHz, and the selective ^{27}Al pulse before t_2 was 11.5 μ s in duration with a rf amplitude of 22.0 kHz. Other parameters were as for Figure 3, except for **B** the relaxation delay was 5.1 s. Experimental details are given in the SI.

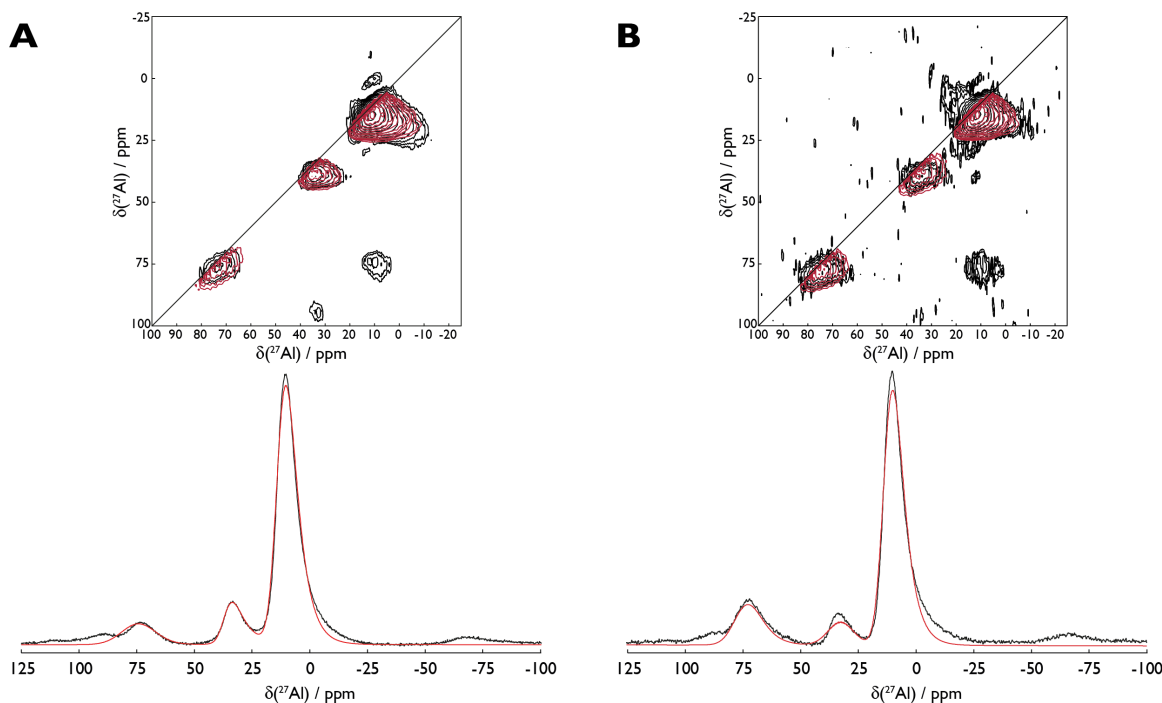


Figure 5. Fits to data using the DMFit package:³² **A** γ -alumina: (top) two-dimensional fit (red) to the DNP-enhanced $\{^1\text{H}\} - ^{27}\text{Al}$ CP-MQMAS spectrum shown in Figure 4A (black), (bottom) one-dimensional fit (red) to the DNP-enhanced $\{^1\text{H}\} - ^{27}\text{Al}$ CPMAS spectrum shown in Figure 3A (black). **B** BaO-modified γ -alumina: (top) two-dimensional fit (red) to the DNP-enhanced $\{^1\text{H}\} - ^{27}\text{Al}$ CP-MQMAS spectrum of BaO-modified γ -alumina shown in Figure 4B (black), (bottom) one-dimensional fit (red) to the DNP-enhanced $\{^1\text{H}\} - ^{27}\text{Al}$ CPMAS spectrum of BaO-modified γ -alumina shown in Figure 6

(black). Further details of the fitting are described in the text and the resulting parameters are shown in Table 1.

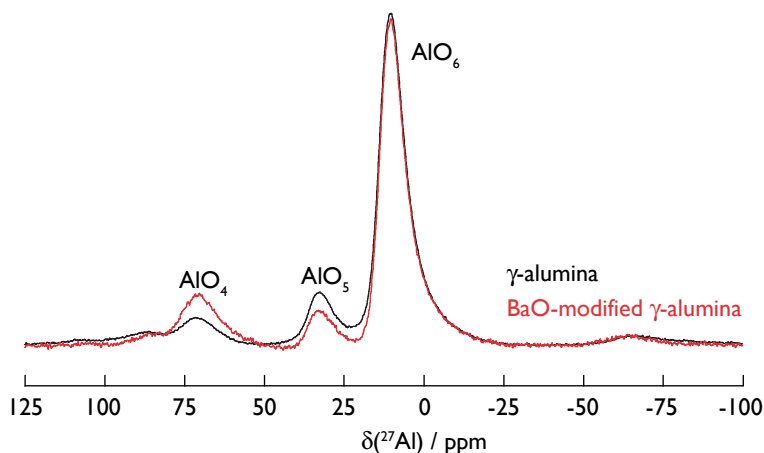


Figure 6. DNP-enhanced $\{^1\text{H}\} - ^{27}\text{Al}$ CPMAS spectrum of BaO-modified γ -alumina and comparison with the corresponding spectrum of unmodified γ -alumina from Figure 3.

The data are normalized to the total spectral integral.

Acknowledgements

The 600 MHz/395 GHZ DNP spectrometer used in this work was purchased with funding from EPSRC's Strategic Equipment Panel (EP/L022524) and the University of Nottingham. MM thanks EPSRC and Johnson Matthey for a PhD Studentship funded under the industrial CASE scheme.

References

- 1 Q. Z. Ni, E. Daviso, T. V. Can, E. Markhasin, S. K. Jawla, T. M. Swager, R. J. Temkin, J. Herzfeld and R. G. Griffin, *Acc. Chem. Res.*, 2013, **46**, 1933–1941.
- 2 A. J. Rossini, A. Zagdoun, M. Lelli, A. Lesage, C. Copéret and L. Emsley, *Acc. Chem. Res.*, 2013, **46**, 1942–1951.
- 3 T. V. Can, Q. Z. Ni and R. G. Griffin, *J. Magn. Reson.*, 2015, **253**, 23–35.
- 4 D. Lee, S. Hediger and G. De Paëpe, *Solid State Nucl. Magn. Reson.*, 2015, **66-67**, 6–20.
- 5 R. I. Hunter, P. A. S. Cruickshank, D. R. Bolton, P. C. Riedi and G. M. Smith, *Phys.*

- Chem. Chem. Phys.*, 2010, **12**, 5752–5756.
- 6 T. F. Kemp, H. R. W. Dannatt, N. S. Barrow, A. Watts, S. P. Brown, M. E. Newton and R. Dupree, *J. Magn. Reson.*, 2016, **265**, 77–82.
 - 7 M. Rosay, L. Tometich, S. Pawsey, R. Bader, R. Schauwecker, M. Blank, P. M. Borchard, S. R. Cauffman, K. L. Felch, R. T. Weber, R. J. Temkin, R. G. Griffin and W. E. Maas, *Phys. Chem. Chem. Phys.*, 2010, **12**, 5850–5860.
 - 8 W. R. Grüning, A. J. Rossini, A. Zagdoun, D. Gajan, A. Lesage, L. Emsley and C. Copéret, *Phys. Chem. Chem. Phys.*, 2013, **15**, 13270.
 - 9 R. L. Johnson, F. A. Perras, T. Kobayashi, T. J. Schwartz, J. A. Dumesic, B. H. Shanks and M. Pruski, *Chem. Commun.*, 2016, **52**, 1859–1862.
 - 10 F. A. Perras, U. Chaudhary, I. I. Slowing and M. Pruski, *J. Phys. Chem. C*, 2016, **120**, 11535–11544.
 - 11 T. Kobayashi, F. A. Perras, U. Chaudhary, I. I. Slowing, W. Huang, A. D. Sadow and M. Pruski, *Solid State Nucl. Magn. Reson.*, 2017, **87**, 38–44.
 - 12 F. A. Perras, J. D. Padmos, R. L. Johnson, L.-L. Wang, T. J. Schwartz, T. Kobayashi, J. H. Horton, J. A. Dumesic, B. H. Shanks, D. D. Johnson and M. Pruski, *J. Am. Chem. Soc.*, 2017, **139**, 2702–2709.
 - 13 M. A. Hope, D. M. Halat, P. C. M. M. Magusin, S. Paul, L. Peng and C. P. Grey, *Chem. Commun.*, 2017, **53**, 2142–2145.
 - 14 G. Busca, in *Advances in Catalysis*, ed. F. C. Jentoft, Academic Press, 2014, vol. 57, pp. 319–404.
 - 15 N. S. Barrow, A. Scullard and N. Collis, *Johnson Matthey Technol. Rev.*, 2016, **60**, 95–102.
 - 16 M. Shelef and H. Gandhi, *Platin. Met. Rev.*, 1974, **18**, 2–14.
 - 17 M. Haouas, F. Taulelle and C. Martineau, *Prog. Nucl. Magn. Reson. Spectrosc.*, 2016, **94-95**, 11–36.
 - 18 H. D. Morris and P. D. Ellis, *J. Am. Chem. Soc.*, 1989, **111**, 6045–6049.
 - 19 D. Coster, A. L. Blumenfeld and J. J. Fripiat, *J. Phys. Chem.*, 1994, **98**, 6201–6211.
 - 20 H. J. Kim, H. C. Lee and J. S. Lee, *J. Phys. Chem. C*, 2007, **111**, 1579–1583.
 - 21 D. Lee, N. T. Duong, O. Lafon and G. De Paëpe, *J. Phys. Chem. C*, 2014, **118**, 25065–25076.
 - 22 J. H. Kwak, J. Z. Hu, D. H. Kim, J. Szanyi and C. H. F. Peden, *J. Catal.*, 2007, **251**, 189–194.
 - 23 R. Wischert, P. Florian, C. Copéret, D. Massiot and P. Sautet, *J. Phys. Chem. C*, 2014, **118**, 15292–15299.

- 24 Y. Rozita, R. Brydson, T. P. Comyn, A. J. Scott, C. Hammond, A. Brown, S. Chauruka, A. Hassanpour, N. P. Young, A. I. Kirkland, H. Sawada and R. I. Smith, *ChemCatChem*, 2013, **5**, 2695–2706.
- 25 V. Vitzthum, P. Mieville, D. Carnevale, M. A. Caporini, D. Gajan, C. Copéret, M. Lelli, A. Zagdoun, A. J. Rossini, A. Lesage, L. Emsley and G. Bodenhausen, *Chem. Commun.*, 2012, **48**, 1988.
- 26 A. Zagdoun, G. Casano, O. Ouari, M. Schwarzwälder, A. J. Rossini, F. Aussenac, M. Yulikov, G. Jeschke, C. Copéret, A. Lesage, P. Tordo and L. Emsley, *J. Am. Chem. Soc.*, 2013, **135**, 12790–12797.
- 27 J.-B. d'Espinose de la Caillerie, C. Fretigny and D. Massiot, *J. Magn. Reson.*, 2008, **192**, 244–251.
- 28 H. Kraus, M. Muller, R. Prins and A. Kentgens, *J. Phys. Chem. B*, 1998, **102**, 3862–3865.
- 29 S. E. Ashbrook and S. Wimperis, *J. Magn. Reson.*, 2000, **147**, 238–249.
- 30 G. Czjzek, J. Fink, F. Gotz, H. Schmidt, J. Coey, J. P. Rebouillat and A. Lienard, *Phys. Rev. B*, 1981, **23**, 2513–2530.
- 31 G. Le Caer and R. A. Brand, *J. Phys.-Condens. Mat.*, 1998, **10**, 10715–10774.
- 32 D. Massiot, F. Fayon, M. Capron, I. King, S. Le Calve, B. Alonso, J. O. Durand, B. Bujoli, Z. H. Gan and G. Hoatson, *Magn. Reson. Chem.*, 2002, **40**, 70–76.
- 33 J. H. Kwak, J. Hu, D. Mei, C.-W. Yi, D. H. Kim, C. H. F. Peden, L. F. Allard and J. Szanyi, *Science*, 2009, **325**, 1670–1673.